Arabian Journal of Geosciences (2021) 14: 325
https://doi.org/10.1007/s12517-021-06576-8

ORIGINAL PAPER

Comprehensive analysis of cloudiness over Iran with CloudSat data

Elham Ghasemifar[1] · Jorge Eiras-Barca[2] · Mohammad Rezaei[1] · Luis Gimeno[2] · Raquel Nieto[2]

Received: 21 August 2020 / Accepted: 19 January 2021 / Published online: 16 February 2021

Abstract

The spatial distribution of different clouds has a significant effect on the supply of water resources, especially in countries with water shortages. Eight-years CloudSat 2B-CLDCLASS data for extended winters (October to March) from 2010 to 2017 has been used here to analyze the characteristics of the cloud cover over Iran. The results show that cirrus-type clouds are the most abundant, with a presence of 28%, followed by altostratus, with a presence of 22.5%. High variability in spatial distribution has also been observed. The most frequent type of cloudiness associated with each region of the country is detailed in this article. The average height of each type of cloudiness observed is also analyzed, being, in the case of the two most frequent types, 10.47 km for cirrus and 7.36 for altostratus. The greatest contribution to rainfall was, however, made by the nimbostratus, with a rate close to 45%. Behind them, stratocumulus, altocumulus, and clouds associated with deep convection show rates of 23.8%, 9.8%, and 8.33%.

Keywords Cloud types · Precipitation · CloudSat · Iran

Introduction

The placing of the satellites in orbit has enabled precise and regular monitoring of cloud coverage over a region of interest (e.g., Saunders and Kriebel 1988; Rossow and Schiffer 1991, 1999; Ackerman et al. 1998; Wang and Sassen 2007). Since cloudiness plays a very relevant role in the radiation balance (e.g., Delgado-Bonal et al. 2020; Collow and Miller 2016), it is also fundamental for the detailed description of the hydrological cycle and the water balance.

The cloudiness distribution is known to show, in general terms, a high variability in its distribution both in time and space and along the different vertical levels (e.g., Benas et al. 2020; Ghasemifar et al. 2018a; King et al. 2013; Subrahmanyam and Kumar 2013; Kahn et al. 2008; Meerkötter et al. 2004; Rossow et al. 1989). Possible changes in these characteristics would lead to changes in the energy balance (e.g., L'ecuyer et al. 2019) and therefore in the fields of precipitation (e.g., Ghasemifar et al. 2018b; Manea et al. 2016). The countries surrounding the Arabian Peninsula are well-known for their scarce water resources. In these kind of regions, it is therefore essential to maintain an updated and detailed study of the characteristics of local cloudiness, since it will play a critical role for agriculture and water supply for the population.

The literature has numerous studies that analyze the characteristics of cloud cover over almost the entire planet, making use mostly of surface observations and passive/optic data (e.g., Gao et al. 2019 in East China, Eastman et al. 2011 over the oceans, or Li et al. 2006 over Tibetan Plateau). However, the use of satellite-mounted active radar tools has now proved much more convenient, as they provide, among other things, a detailed analysis of vertical profiles (Hong and Gourley 2015). In particular, the analyses carried out with CloudSat on different regions of the planet have yielded very positive results in recent years (e.g., Kukulies et al. 2019; Jiang et al. 2018; Li et al. 2014; Behrangi et al. 2012; Subrahmanyam and Kumar 2013; Sassen and Wang 2008). With the comprehensive cloud profile information provided by CloudSat data, it is found that (i) the maximum (minimum) cloud fraction corresponded to deep convective clouds (the transition from shallow to deep convective regimes), occurring at sea surface

Responsible editor: Zhihua Zhang

✉ Elham Ghasemifar
elham.ghasemifar@modares.ac.ir

[1] Satellite Climatology, Department of Physical Geography, Tarbiat Modares University, Tehran, Iran

[2] Environmental Physics Laboratory (EPhysLab), CIM-UVIGO, Universidade de Vigo, Ourense, Spain

temperatures (SST) of 303 K (299 K) (Behrangi et al. 2012). (ii) The maximum (minimum) horizontal length is recorded for nimbostratus (cumulus), while the maximum (minimum) cloud thickness is found in coincidence with the presence of deep convective (stratocumulus) cloudiness (Guillaume et al. 2018). (iii) High clouds are more likely to coexist with other cloud types, while Stratocumulus, nimbostratus, and convective tend to be individual features (Li et al. 2014). (iv) Stratocumulus (cirrus) clouds exert the largest cooling (warming) effect of about −8.2 (2) W/m^2 (L'ecuyer et al. 2019). The results could improve the information provided by passive data in the past. The satellite data also provides more explicit precipitation information, which is crucial in the differentiation between precipitation and non-precipitation clouds and cloudiness related to the formation of baroclinic structures (Xu et al. 2019; Naud et al. 2015).

Iran (Fig. 1a) is located in an arid and semi-arid region of Southwest Asia, in an extensive domain that covers the latitude range between 25°N and 40°N and in a longitude range between 45°E and 60°E. There are two air masses that mainly affect the region: on the one hand, a mass that transports humidity from the Mediterranean Sea and, on the other hand, another drier air mass that transports air from the North and Northeast, under the action of the Siberian anticyclone, particularly in the cold months. The wide extension of Iran allows it to have different climatic regimes although in global terms, it is characterized by having a wet season, coinciding with the boreal winter, in which almost 90% of the precipitation occurs (Darand and Mansouri Daneshvar 2014). The region with the highest number of rainy days is the Caspian Coast, located in the north of the country, which has more than 120 days of rain per year. In contrast, the region with the fewest days of rainfall is the southeast and south of the country, with an average of 20 days of rainfall per year (Alijani and Harman 1985). The mechanisms leading to precipitation are also accepted to be well different among

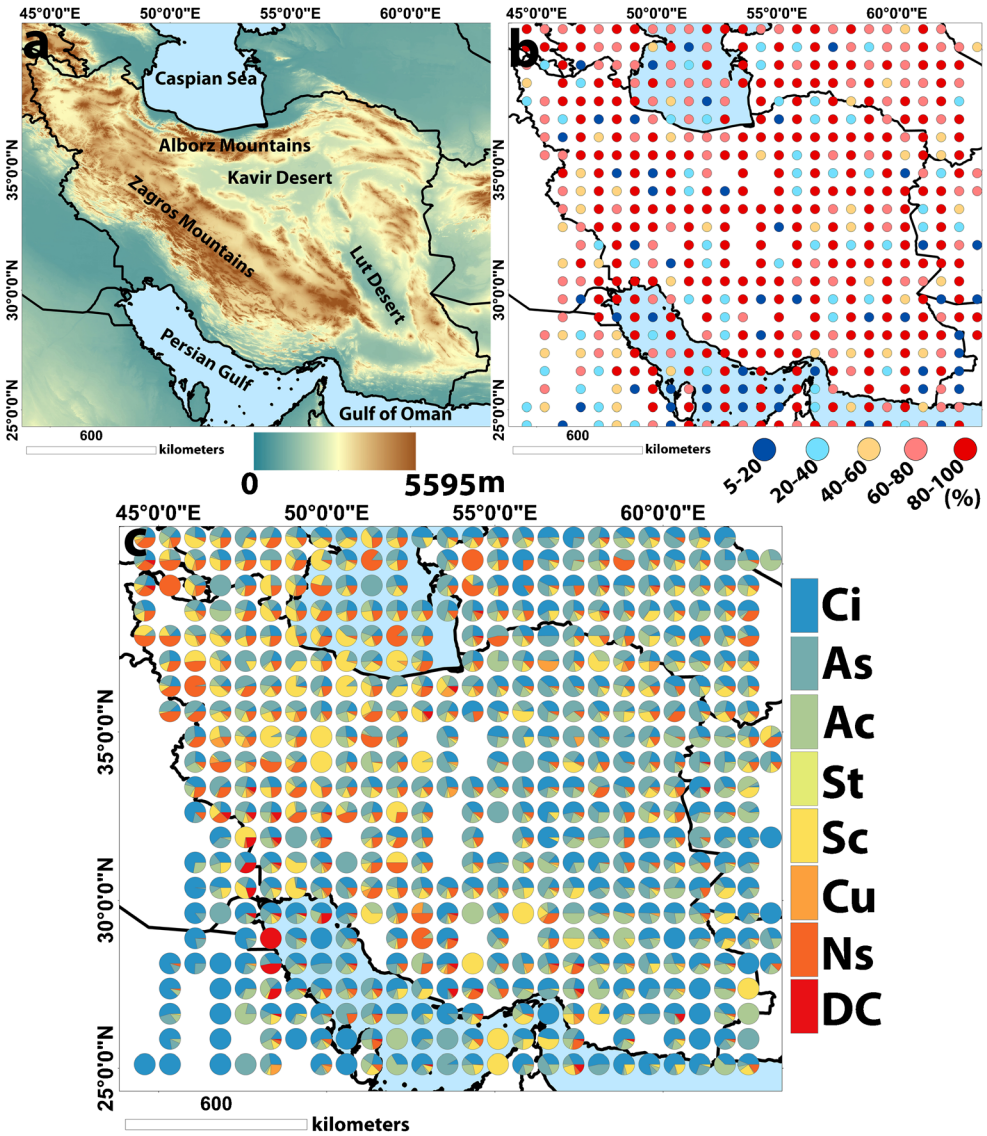

Fig. 1 (**a**) Elevation map of Iran. (**b**) The total cloudiness. (**c**) Average contribution of different cloud types to total cloudiness

northern and southern areas. While the influence of the westerlies, surface heating, and maritime impacts are considered to be the most important triggering in northern Iran, the southern latitudes are mostly affected by upper-level disturbances (Alijani and Harman 1985). Overall, the altitude does only account for 10% of the precipitation variability (Alijani et al. 2008). In a study focusing on Iran, Ghasemifar et al. (2018a) showed that latitude, vegetation, and altitude can explain local cloud variability by up to 63%, 32%, and 28%, respectively. It was also shown that the greatest variability occurs in fall, when the region is more influenced by air mass intrusions. Using optical data, Moderate Resolution Imaging Spectroradiometer (MODIS), and data from the International Satellite Cloud Climatology Project (ISCCP), Ghasemifar et al. (2018b) has shown that altostratus, stratocumulus, and nimbostratus, having the highest frequency of occurrence in cold months, recorded the maximum precipitation.

Despite the existence of studies on Iran that have attempted to analyze its cloudiness with optical instruments mounted on satellites, there is, to best of our knowledge, no study that makes use of satellite radar data for this purpose. The main objective of this article is to show the results of the analysis of the characteristics of cloudiness over Iran, obtained with this data source that has proved to be a useful and accurate source of information.

Data and methods

CloudSat cloud profiling radar (CPR) data (Stephens et al. 2008) from A-train constellation data, collected since April 2006, at a frequency of 94 GHz and an altitude of about 700 km has been used here. The track of the satellite overpasses the same location every 16 days and provides a resolution of 1.4 km in cross-track and 1.8 km in along-track. 3.3 μs pulses provide information at 240-m vertical resolutions from the surface to 30 km. Particularly, in this study, we make use of the 2B-CLDCLASS product of CloudSat level 2 observations (Wang and Sassen 2007, Sassen and Wang 2008), restricted to the extended winter (from October to March) throughout 2010–2017 over Iran. CloudSat overpasses our region of interest between 08:00 AM and 09:30 AM UTC in the descending node and between 08:30 PM and 10:00 PM UTC in the ascending node.

The first approaches of distinguishing between different cloud types, e.g., the International Satellite Cloud Climatology Project (ISCCP), used cloud optical depth and cloud top pressure by combining data collected by passive satellite and summarized them in the C, D, and H series (Rossow and Schiffer 1991, 1999; Rossow 2017). Wang and Sassen (2001) developed an algorithm using data collected by active instruments (radar and lidar) and passive instruments (infrared and microwave radiometers) to cloud classification. The 2B-CLDCLASS algorithm makes use of 2B-GEOPROF, MODIS, and other additional data to provide cloud properties such as height, phase, radar reflectivity, and cloud thickness. First, a cloud mask is used to find a cloud cluster. Once a cloud cluster is found, all the variables of interest are observed or derived. Then, a fuzzy method is used in the algorithm to classify observations into eight classes: cirrus [Ci], altostratus [As], altocumulus [Ac], stratus [St], stratocumulus [Sc], cumulus [Cu], nimbostratus [Ns], and deep convective [DC] clouds (i.e., cumulonimbus).

The procedure that has been applied here to extract the different cloud types is as follows:

1. CloudSat data has been extracted in a regular 0.75 × 0.75 degree grid raster.
2. For every grid point (625), the occurrence of each cloud type has been obtained.
3. The number of occurrences has been divided by the total cloud types of each grid.
4. The base and top height, together with the mean height, have been obtained for further analysis.
5. The precipitation/non-precipitation rates have been obtained based on the total number of grids that recorded precipitation.

Results

Cloud type distribution spatial patterns

The analysis of the total cloud fraction (Fig. 1b) showed that the minimum mean cloud cover fraction (lower than 20%) has been located in the southeastern, southern, and central regions of the country. The maximum total cloud fraction (greater than 80%) has been located on the southern coast of the Caspian Sea (especially the Western Coast) and over Zagros mountains. Overall, the cloud cover fraction is 5% greater in latitudes below 30 degrees, when compared to latitudes above this value due to much more contribution of high clouds.

Figure 1c shows the average contribution of each cloud type to the total cloudiness (October to March, 2010–2017). As shown, the largest contribution in the south and southeast is made by [Ci] and [As], while in northern mountainous areas, all types tend to be relevant. Table 1 shows the relative contribution of each cloud type to total cloudiness. [Ci] and [As] make more than half of the contribution both above and below 30°N. Particularly, [Ci] are the most frequent cloud type, with great contribution in both cases, especially below 30°N, where almost half of the total cloudiness is corresponding to this type.

Figure 2 shows the mean monthly spatial distribution of each cloud type considered in this analysis. As it was already

Table 1 Contribution of each cloud type to total cloudiness in Iran for extended winter months

Type	Contribution below 30 °N	Contribution above 30 °N
Cirrus [Ci]	43.33%	21.48%
Altostratus [As]	15.32%	25.8%
Altocumulus [Ac]	14.74%	10.08%
Stratus [St]	0.008%	0.01%
Stratocumulus [Sc]	9.76%	14.12%
Cumulus [Cu]	1.43%	1.62%
Nimbostratus [Ns]	4.44%	12.55%
Deep convective [DC]	2%	0.57%
Total	91.03%	86.23%

discussed, [Ci] clouds are by far the most prevalent, especially in the southern and central sectors of the country. Particularly, in certain locations, [Ci] clouds are responsible for more than 80% of the monthly contribution to total cloudiness. [As] clouds are the second most frequent type of cloudiness. The greater presence of this type of cloudiness is found in the Northeastern, Eastern, and Central regions, as well as above the Caspian Sea. Its greater occurrence is found to be located over the central region, and almost no occurrence is found over the southern latitudes. Northeastern, eastern, southern, and central regions of Iran showed the maximum frequency of [Ac], but this type of cloud showed negligible occurrence in western Iran, from 45°E to 50°E. On the contrary, the [St] have a negligible presence in the entire domain. Only a slight amount of this type of cloud can be seen in the central regions, during November and February. [Sc] show the highest frequency of occurrence over the Persian and Oman Gulfs, the Caspian Sea and its coastal regions, and northwestern and central regions. [Cu] cloudiness is more frequent (up to 50 percent) close to Caspian and southern seas. [Ns] clouds are more frequent over northwestern zones, the Caspian Sea, the coastal regions, and over Zagros and Alborz mountains. It is also interesting to comment on the role played by the cloudiness associated with deep convection [DC], whose presence is mainly located over the Persian Gulf, except for the month of October, where some presence is also observable in the vicinity of the Caspian Sea.

Cloud type distribution time series

Figure 3 shows the mean time series of zonal (first column) and meridional (second column) means associated with each type of cloud. In this figure, the conclusions already discussed about the dominant detection of each cloud types are verified again. Particularly, it is clearly observed that increases in latitude are correlated with increases in the detection of [As], [Sc], and [Ns], while [Ci] shows the reverse pattern. The third column provides information regarding the mean height location of each cloud type. In general terms, each type of cloud has the expected behavior. The [Ci], which are the most abundant type of cloud, is restricted to the upper levels of the troposphere, between the 6-km level and the 14-km level. The [As], which are considered medium-level clouds, can be observed at all vertical levels. The rest of the cloud types shown are mainly restricted to the lower levels.

Figure 4 shows the coefficient of variation (CV) associated with each cloud type. High values of this CV can be consistently found in northwestern regions in the case of the [Ci] and in southern regions in the case of [Sc], [Cu], [Ns], and [DC], denoting a high variability. By contrast, consistent low values of the CV can be found in the southeast for the [Ci] and in northern latitudes for [As], [Ac], and [Sc] mostly.

Figure 5 shows the interannual time series of mean cloud fractions for each cloud type. Even though some cloud types—particularly remarkable is the case of the cirrus—show some important variability, no specific trends are detected here. Thus, conclusions that can be taken from this figure are coincident with those already obtained in Table 1.

Vertical characteristics of each cloud type

Figure 3 (right panel) already provided information on the average height associated with each type of cloud. However, since critical information—such as the thermodynamic phase of the suspended water microparticles, the type of precipitation, as well as the probability of associating hail in the precipitation—is highly dependent on the vertical structure of the cloud, we consider it appropriate to extend the information on the vertical characteristics of each type, in Table 2. Well-known characteristics of each cloud types, most of them already discussed in this article, are particularly clearly shown in the table for each month. For example, the vertical development of [DC] clouds, with heights of close to 13 km, may be observed every month. Also the high-cloud nature of the [Ci] or the fact that even though [As] are considered to be mid-clouds, the min base height is close to the ground level for every single month in the analysis.

Associated precipitation

Figure 6 shows the relative contribution of each type of precipitation to precipitation/non-precipitation cloudiness. The first conclusion that can be drawn from this figure is that the results are mostly consistent between the different months of the extended winter. On the one hand, in each of the months, [Ci] and [As] may be clearly considered as non-precipitation clouds. On the other hand, [Ns] and [DC] can be clearly considered as precipitation clouds. [Ac], [Sc], and [Cu] show a

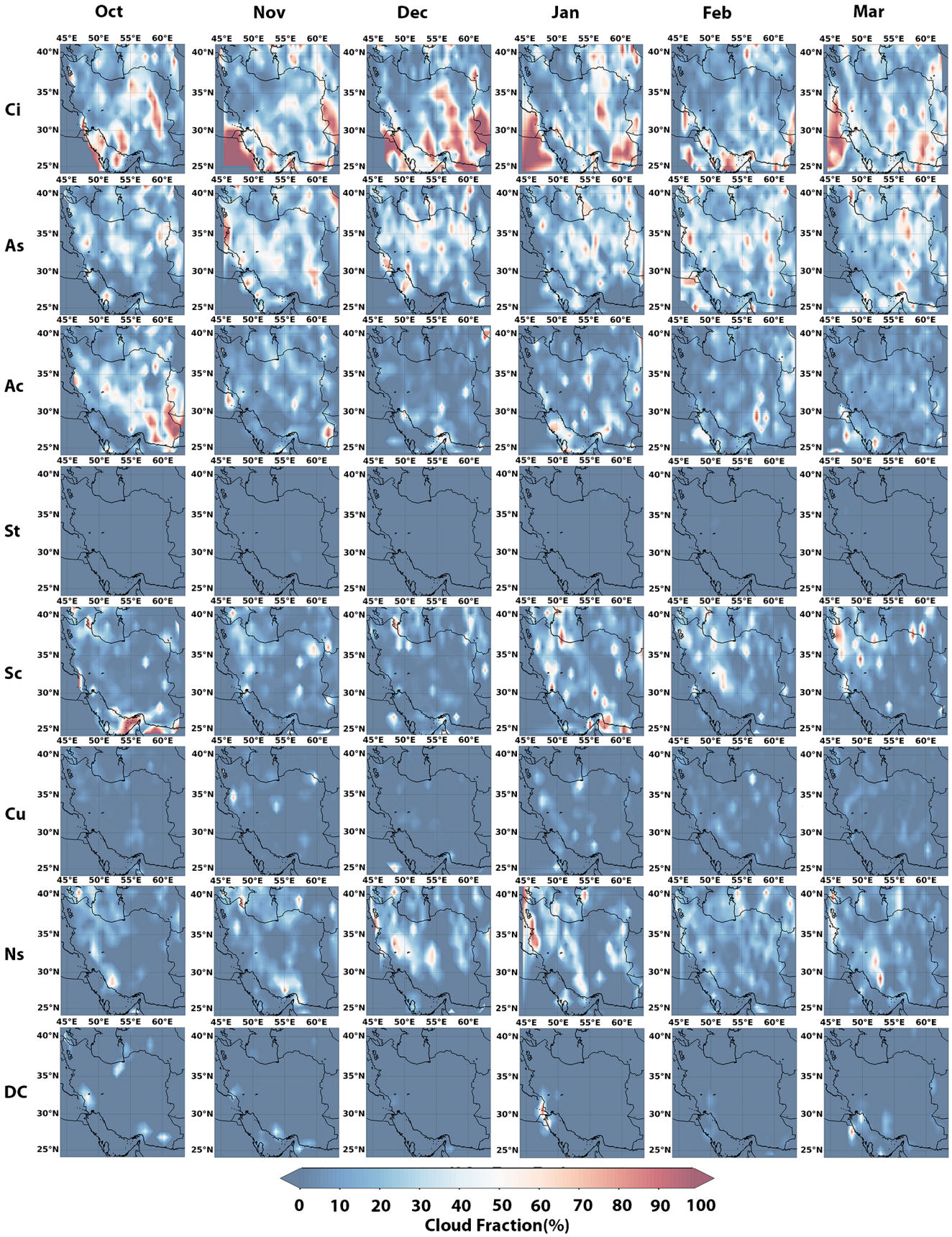

Fig. 2 Mean monthly distribution associated with each cloud type. Note that at any given point, the sum may be greater than 100%, as there is a possibility that two types of clouds may coexist simultaneously at different vertical levels

hybrid behavior. In general terms, these conclusions were expected and are in coincidence with what has already been observed in many other regions of the world. Table 3 shows the Spearman correlation between these cloud types and rain rate observed by CloudSat. The three most non-precipitation clouds show negative correlations with rain rate, but, as expected, precipitation clouds clearly show a positive correlation with rain rate.

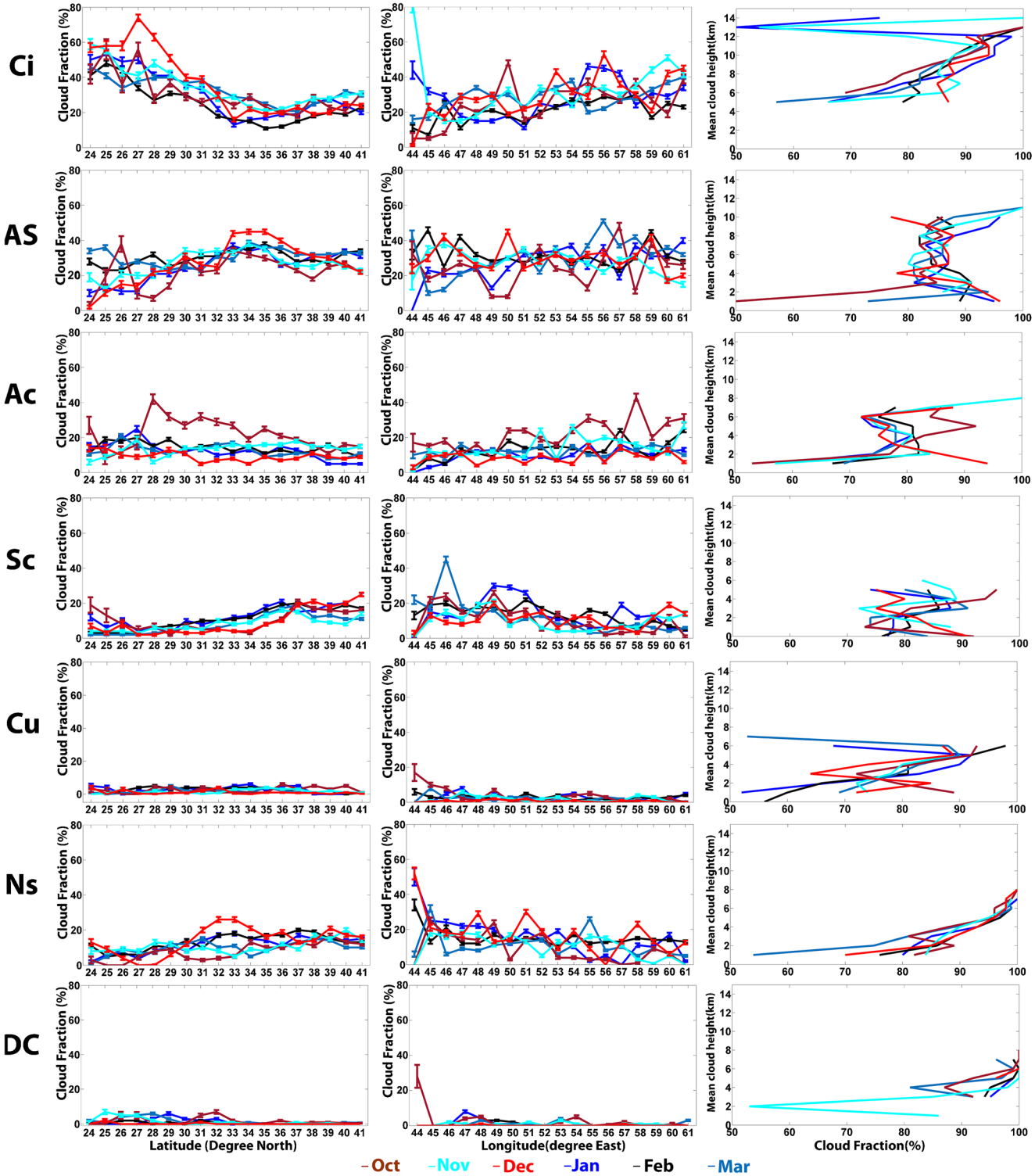

Fig. 3 Time series of zonal (first column) and meridional (second column) mean cloud fractions corresponding to each cloud type over Iran. Third column shows the average height associated with each type of cloud

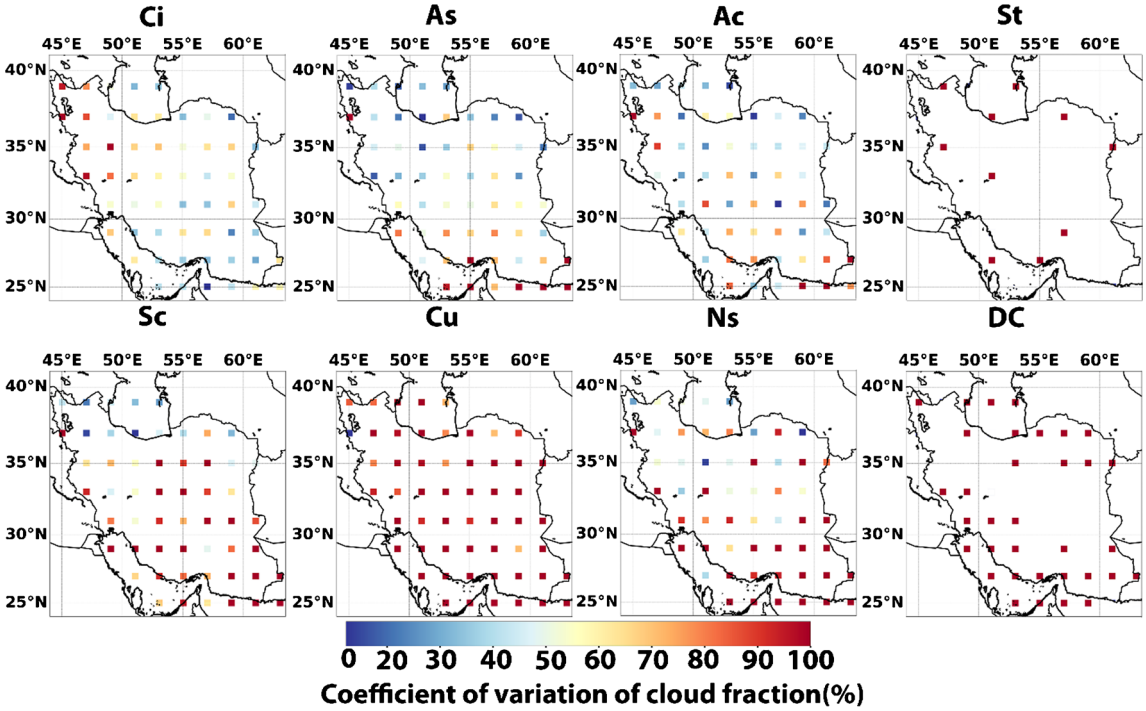

Fig. 4 Coefficient of variation for different cloud types over Iran in October to March (2010 to 2017)

Finally, Fig. 7 shows the location of the base height and top height of each type of cloud, depending on whether these values have been recorded along with the detection of precipitation. In general terms, the base (top) height of precipitation clouds is lower (higher) than in non-precipitation clouds. This figure should be analyzed together with Fig. 6a, since, for example, for the case of [As], the value of the base height for the case of non-precipitation cloud will be much more representative, since this type of cloud rarely leads to precipitation.

Discussion

The literature has proven the numerous advantages of CloudSat CPR. However, some weaknesses have also been reported. Overall, CloudSat radar underestimates cloud presence by 4.2% and 1% compared to surface and ISCCP data, respectively (Sassen and Wang 2008), and 4.5% compared to 2B-CLDCLASS-Lidar (Li et al. 2014), except for altostratus and nimbostratus. Behrangi et al. (2012) also pointed out two issues with 2B-CLDCLASS data:

i. Due to potential high values of contamination, from the surface to ~ 1 km, the product may not able to accurately estimate the observation of stratus and stratocumulus.
ii. Thin clouds may be omitted in cloud classification due to the lower sensitivity of radar to high thin clouds when compared to Lidar. According to Sassen and Wang (2008), cirrus may be underestimated by CloudSat due to insufficient size of hydrometeors to be properly detected by the systems.

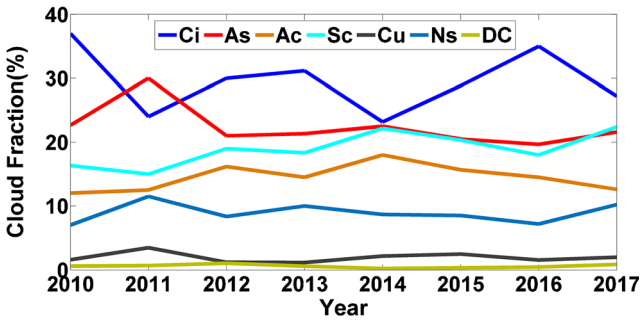

Fig. 5 Time series of spatially integrated annual cloud fraction for each cloud type

The study presented here addresses the weaknesses observed in Ghasemifar et al. (2018b), since CPR is not being affected by surface albedos, temperature, and elevation that may interfere with proper detection of cirrus in cold months when you are using optical instruments (Sassen et al. 2008) as such used by MODIS.

The warmest regions in Iran during winter are the South and Southwest areas (with SST higher than 301 K; Ghasemifar et al. 2019). These are also areas where the maximum occurrence of cirrus cloudiness is observed. This is consistent with the idea that convergence in low and mid-levels, in coincidence with SST higher than 301 K, is a favorable condition to the formation of this type of cloudiness (Behrangi et al. 2012; Peng et al. 2014; Guo and Zhou 2015).

Table 2 Characteristics of the height (km) of different cloud types from October to March over Iran during 2010 to 2017

		Ci	As	Ac	St	Sc	Cu	Ns	DC
Oct	Min base ht	5	0.4	0.5	1.6	0.4	0.3	0.3	0.4
	Max base ht	14.4	13.3	9.5	3.1	6.7	10.9	12.6	13.3
	Mean top ht	10.21	9.1	5.8	2.5	3.3	5.1	8.4	10.87
Nov	Min base ht	5	0.5	0.4	2.8	0.36	0.37	0.36	0.37
	Max base ht	17.4	14	9.9	5.9	6.6	9.2	12.8	14.32
	Mean top ht	10	8.7	5.4	5.2	3.6	4.5	8	10.62
Dec	Min base ht	4.7	0.5	0.5	2	0.35	0.5	0.3	0.5
	Max base ht	18.4	12.8	8.4	3.3	6.7	9.2	13	11.68
	Mean top ht	9.9	8.53	5.3	3.7	2.7	5.4	7.5	10.74
Jan	Min base ht	5	0.6	0.4	2	0.35	0.4	0.3	0.3
	Max base ht	14.52	12	8.4	3.3	6.79	9.47	11.27	10.81
	Mean top ht	9.48	7.7	5.6	3.76	2.83	5.7	7.12	9.62
Feb	Min base ht	4.7	0.6	0.4	1.28	0.4	0.3	0.35	0.35
	Max base ht	18	12.5	8.9	5	6.7	10.13	12.24	11.63
	Mean top ht	9.6	8.5	5.3	3	3.17	5.46	7.8	9.5
Mar	Min base ht	5	0.4	0.5	1.3	0.3	0.4	0.3	0.3
	Max base ht	17.32	13.7	9.1	5.5	7.1	10.14	13.5	12.8
	Mean top ht	10	8.8	5.5	4.6	3.2	6	6.9	3.4

The spatial distribution of altostratus showed in this manuscript is in agreement to that already reported by L'ecuyer et al. (2019), Naud et al. (2015), Li et al. (2014), and Sassen and Wang (2008), that already reported the high occurrence of these clouds over mid- and high latitudes in Iran, mostly due to frictional and blocking effects of Zagros and Alborz mountains. The key role played by the Tibetan Plateau in the potential formation of altostratus has also been discussed by Yu et al. (2004).

Altocumulus clouds are also frequent in deep convection systems (Naud et al. 2015; Li et al. 2014) and are frequently observed in these kind of subtropical regions (Li et al. 2014). In this regard, the values reported here are in agreement with those that could be expected. The spatial distribution of stratucumuls over Iran that we report here has been also stated by Ghasemifar et al. (2018b). These type of clouds are favored by temperature inversions and large-scale subsidence and high stability (Wood 2012, 2015; Li and Gu 2006). In lower latitudes, they tend to be formed in the downward branches of Hadley cell, while in the mid-latitudes, they are mostly associated with ridge in planetary waves (Wood 2015).

Factors including the ascent strength and temperature contrasts across the cold fronts are favorable for nimbostratus formation (Naud et al. 2015). Westerlies disturbances, including cyclonic circulation, favor the detection of frontal systems over Iran's cold months, particularly over the northern region and Zagros (Alijani and Harman 1985). Mountainous regions force the westerlies to the low-level convergence and mid-level divergence for a steady lifting in the lower troposphere and the subsequent formation the cloud (Yu et al. 2004).

According to previous studies that showed a strong diurnal cycle (Gao et al. 2019) and strong interannual and seasonal variation (Eastman et al.,2011), we report here a variability of total cloud fraction between 0 and 60% which is related to the different characteristics of air masses penetrating Iran,

Table 3 Spearman correlations between rain rate and different cloud types used considered in the analysis (p <0.01 are labeled with**)

Month	Ci	As	Ac	St	Sc	Cu	Ns	DC
Oct	−0.23**	−0.20**	−0.17**	−0.01	0.28**	0.26**	0.48**	-
Nov	−0.28**	−0.09**	−0.08**	-	0.10**	0.19**	0.18**	0.15**
Dec	−0.28**	−0.13**	−0.04**	-	0.31**	0.06**	0.34**	0.09**
Jan	−0.19**	−0.18**	0.02	-	0.10**	0.31**	0.26**	0.15**
Feb	−0.25**	−0.09**	−0.15**	-	0.09**	0.16**	0.58**	0.21**
Mar	−0.21**	−0.20**	−0.04**	-	0.12**	0.10**	0.46**	0.31**

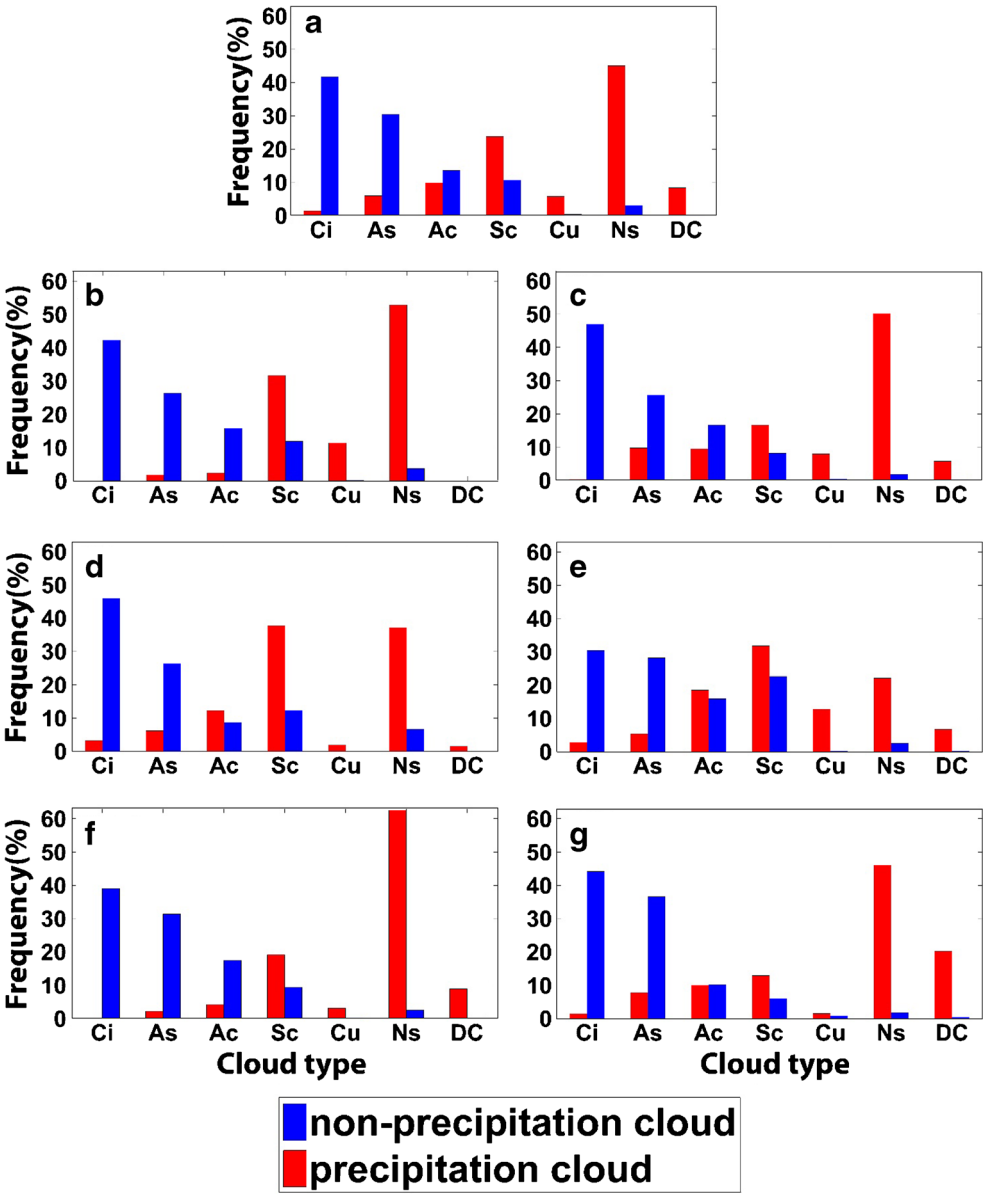

Fig. 6 Monthly classification of each cloud type in terms of associated precipitation: (**a**) the average values, (**b**) to (**g**) represent the values for Oct to Mar, respectively

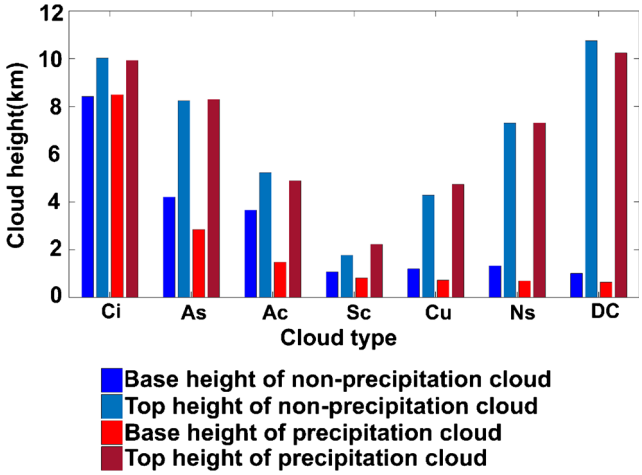

Fig. 7 Base and top height of the most important cloud types classified according to coincidence with precipitation

particularly in fall and winter months (Ghasemifar et al. 2018a). Regarding the cloud heights, previous studies showed that cirrus have the highest mean base and top height in close to 5 km and 18 km, respectively (Sassen et al. 2008; Xu et al. 2019). These results are in agreement to those presented in this manuscript.

Finally, the distribution of (non)precipitation cloudiness presented here is similar and in agreement with that reported by the bulk of the literature (e.g., Sassen and Wang 2008 globally; Xu et al. 2019 in eastern China; Ghasemifar et al. 2018b in Iran; Manea et al.2016 in Romania). In general terms, the base height of precipitation clouds is up to 1 km lower than those in non-precipitation clouds. Precipitation clouds are mostly located below 3 km as reported by Xu et al. (2019) because of the decreasing trend of temperature and water vapor concentration with height (Yue et al. 2013).

Conclusions

This work provides a comprehensive analysis of the cloud characteristics over Iran by using 8 years of CloudSat CPR (2B-CLDCLASS) data. The results show a significant variability among the different regions of the country, being the most common cloud type for each region as follows:

1. Cirrus clouds over the southeastern area
2. Altostratus clouds over the central regions and some areas in the north
3. Altocumulus over eastern longitudes and some areas in the south
4. Stratocumulus, Cumulus, and deep convection cloudiness over seas and coastal regions
5. Nimbostratus over mountainous areas

Cirrus show the highest top height and vertical location variability—from 4.9 to 16.67 km—followed by altostratus, from 0.5 to 13 km, and deep convection cloudiness, 0.37 to 12.5 km. The lowest top height has been found for stratus—from 1.8 to 4.5 km—and stratocumulus, from 0.36 to 6.7 km.

Cirrus and altostratus behave mostly as non-precipitation clouds over Iran. In contrast, nimbostratus, stratocumulus, and deep convection cloudiness behave mostly as precipitation clouds. These results show a certain but slight variability among the extended winter months. The greatest contribution to rainfall was made by the nimbostratus, with a rate close to 45%. Behind them, stratocumulus, altocumulus, and clouds associated with deep convection show rates of 23.8%, 9.8%, and 8.33%.

Since these analyses are purely based on observations, we consider it to be reliable. However, it has been reported in the literature that CPR tends not to detect thinner clouds. Thus, cirrus and stratus results reported here are subject to a certain uncertainty. Lidar data (e.g., CALIPSO) may be used in the future to improve this weakness. Additionally, this analysis is limited to the extended winter—cold—months. It is the authors' intention to complete this study in the future, making use of various data sources, and for the entire year.

Acknowledgements The authors are gratefully thankful to the CloudSat 2B-CLDCLASS team to providing this dataset.

References

Ackerman SA, Strabala KI, Menzel WP, Frey RA, Moeller CC, Gumley LE (1998) Discriminating clear sky from clouds with MODIS. J Geophys Res Atmos 103(D24):32141–32157

Alijani B, O'Brien J, Yarnal B (2008) Spatial analysis of precipitation intensity and concentration in Iran. Theor Appl Climatol 94:107–124

Alijani B, Harman JR (1985) Synoptic climatology of precipitation in Iran. Ann Am Assoc Geogr 75(3):404–416

Behrangi A, Kubar T, Lambrigtsen B (2012) Phenomenological description of tropical clouds using CloudSat cloud classification. Mon Weather Rev 140:3235–3249

Benas N, Meirink JF, Karlsson KG, Stengel M, Stammes P (2020) Satellite observations of aerosols and clouds over southern China from 2006 to 2015: analysis of changes and possible interaction mechanisms. Atmos Chem Phys 20:457–474

Collow ABM, Miller MA (2016) The seasonal cycle of the radiation budget and cloud radiative effect in the Amazon Rain Forest of Brazil. J Clim 29:7703–7722. https://doi.org/10.1175/JCLI-D-16-0089.1

Darand M, Mansouri Daneshvar MR (2014) Regionalization of precipitation regimes in Iran using principal component analysis and hierarchical clustering analysis. Environ Process 1:517–532. https://doi.org/10.1007/s40710-014-0039-1

Delgado-Bonal A, Marshak A, Yang Y, Holdaway D (2020) Analyzing changes in the complexity of climate in the last four decades using MERRA-2 radiation data. Sci Rep 10:922

Eastman R, Warren SG, Hahn CJ (2011) Variations in cloud cover and cloud types over the ocean from surface observations, 1954–2008. J Clim 24:5914–5934

Gao C, Li Y, Chen H (2019) Diurnal variations of different cloud types and the relationship between the diurnal variations of clouds and precipitation in Central and East China. Atmosphere 2019(10):304. https://doi.org/10.3390/atmos10060304

Ghasemifar E, Farajzadeh M, Perry MC, Rahimi YG, Bidokhti AA (2018a) Analysis of spatiotemporal variations of cloud fraction based on geographic characteristics over Iran. Theor Appl Climatol 134:1429–1445. https://doi.org/10.1007/s00704-017-2308-1

Ghasemifar E, Farajzadeh M, Ghavidel Rahimi Y, Bidokhti AA (2018b) Precipitation rate climatology related to different cloud types using satellite imagery over Iran. Arab J Geosci 11:78 (2018). https://doi.org/10.1007/s12517-018-3419-4

Ghasemifar E, Farajzadeh M, Mohammadi C, Alipoor E (2019): Long-term change of surface temperature in water bodies around Iran – Caspian Sea, Gulf of Oman, and Persian Gulf – using 2001 2015 MODIS data. Phys Geogr. https://doi.org/10.1080/02723646.2019.1618231

Guillaume A, Kahn BH, Yue Q, Fetzer EJ, Wong S, Manipon GJ, Hua H, Wilson BD (2018) Horizontal and vertical scaling of cloud geometry inferred from CloudSat Data. J Atmos Sci 75:2187–2197

Guo Z, Zhou T (2015) Seasonal variation and physical properties of the cloud system over southeastern China derived from CloudSat products. Adv Atmos Sci 32(5):659–670. https://doi.org/10.1007/s00376-014-4070-y

Hong Y, Gourley JJ (2015) Radar hydrology principles, models, and applications. CRC Press, Taylor & Francis Group

Jiang JH, Su H, Huang L, Wang Y, Massie S, Zhao B, Omar A, Wang Z (2018) Contrasting effects on deep convective clouds by different types of aerosols. Nature Communications 9:3874. https://doi.org/10.1038/s41467-018-06280-4 www.nature.com/naturecommunications

Kahn BH, Chahine MT, Stephens GL, Mace GG, Marchand RT, Wang Z, Barnet CD, Eldering A, Holz RE, Kuehn RE, and Vane DG (2008) Cloud type comparisons of AIRS, CloudSat, and CALIPSO cloud height and amount. Atmos Chem Phys 8:1231–1248

King MD, Platnick S, Menzel WP, Ackerman SA, Hubanks PA (2013) Spatial and temporal distribution of clouds observed by MODIS onboard the Terra and Aqua Satellites. IEEE transactions on geoscience and remote sensing 51(7):3826–3852. https://doi.org/10.1109/TGRS.2012.2227333

Kukulies J, Chen D, Wang M (2019) Temporal and spatial variations of convection and precipitation over the Tibetan Plateau based on

recent satellite observations. Part I: Cloud climatology derived from CloudSat and CALIPSO. Int J Climatol 39:5396–5412

L'ecuyer TS, Hang Y, Matus AV, Wang Z (2019) Reassessing the effect of cloud type on earth's energy balance in the age of active spaceborne observations. Part I: Top of Atmosphere and Surface. J Clim (32):6197–6217

Li Y, Gu H (2006) Relationship between middle stratiform clouds and large scale circulation over eastern China. Geophys Res Lett 33(9): L09706. https://doi.org/10.1029/2005GL025615

Li Y, Liu X, Chen B (2006) Cloud type climatology over the Tibetan Plateau: a comparison of ISCCP and MODIS/TERRA measurements with surface observations. Geophys Res Lett 33(17). https://doi.org/10.1029/2006GL026890

Li J, Huang J, Stamnes K, Wang T, Yi Y, Ding X, Lv Q, Jin H (2014) Distributions and radiative forcings of various cloud types based on active and passive satellite datasets – Part 1: geographical distributions and overlap of cloud types. Atmos Chem Phys Discuss 14: 10463–10514 https://www.atmos-chem-phys-discuss.net/14/10463/2014/. https://doi.org/10.5194/acpd-14-10463-2014

Manea A, Birsan MV, Tudorache G, Cărbunaru F (2016) Changes in the type of precipitation and associated cloud types in Eastern Romania (1961–2008). Atmos Res 169(2016):357–365. https://doi.org/10.1016/j.atmosres.2015.10.020

Meerkötter R, König C, Bissolli P, Gesell G, Mannstein H (2004) A 14-year European cloud climatology from NOAA//AVHRR data in comparison to surface observations. Geophys Res Lett 31:L15103. https://doi.org/10.1029/2004GL020098

Naud CM, Posselt DJ, van den Heever SC (2015) A CloudSat–CALIPSO view of cloud and precipitation properties across cold fronts over the global oceans. J Clim 25(17):6743–6762

Peng J, Zhang H, Li ZQ (2014) Temporal and spatial variations of global deep cloud systems based on CloudSat and CALIPSO satellite observations. Adv Atmos Sci 31(3):593–603. https://doi.org/10.1007/s00376-013-3055-6

Rossow, W.B. (2017) Climate Data Record Program (CDRP): Climate Algorithm Theoretical Basis Document (C-ATBD) International Satellite Cloud Climatology Project (ISCCP) H-Series, CDRP-ATBD-0872, Asheville, North Carolina, USA, p 179

Rossow WB, Schiffer RA (1991) ISCCP cloud data product. Bull Am Meteorol Soc 72(1):1–20

Rossow WB, Schiffer RA (1999) Advances in understanding clouds from ISCCP. Bull Am Meteorol Soc 80(11):2260–2287

Rossow WB, Gardner LC, Lacis AA (1989) Global, seasonal cloud variations from satellite radiance measurements. Part I: sensitivity of analysis. J Clim 2(5):419–458

Sassen K, Wang Z (2008) Classifying clouds around the globe with the CloudSat radar: 1-year of results. Geophys Res Lett 35:L04805. https://doi.org/10.1029/2007GL032591

Sassen K, Wang Z, Liu D (2008) Global distribution of cirrus clouds from CloudSat/Cloud-Aerosol Lidar and Infrared Pathfinder Satellite Observations (CALIPSO) measurements. J Geophys Res 113: D00A12. https://doi.org/10.1029/2008JD009972

Saunders RW, Kriebel KT (1988) An improved method for detecting clear sky and cloudy radiances from AVHRR data. Int J Remote Sens 9(1):123–150

Stephens GL, Vane DG, Tanelli S, Im E, Durden S, Rokey M, Reinke D, Partain P, Mace GG, Austin R, L'Ecuyer T, Haynes J, Lebsock M, Suzuki K, Waliser D, Wu D, Kay J, Gettelman A, Wang Z, Marchand R (2008) CloudSat mission: performance and early science after the first year of operation. J Geophys Res Atmos 113(D8)

Subrahmanyam KV, Kumar KK (2013) CloudSat observations of cloud-type distribution over the Indian summer monsoon region. Ann Geophys 31:1155–1162

Wang Z, Sassen K (2001) Cloud type and macrophysical property retrieval using multiple remote sensors. J Appl Meteorol Climatol 40(10):1665–1682

Wang Z, Sassen K (2007) Level 2 cloud scenario classification product process description and interface control document, CloudSat Project, A NASA Earth System Science Pathfinder Mission, Version: 5.0

Wood R (2012) Stratocumulus clouds. Mon Weather Rev 140(8):2373–2423

Wood R (2015) Stratus and stratocumulus, in Encyclopedia of Atmospheric Sciences, 2nd ed., vol. 2, edited by G. R. North, J. Pyle, and F. Zhang. Elsevier, pp 196– 200

Xu J, Liu D, Wang Z, Wu D, Yu S, Wang Y (2019) A study of the characteristics of vertical cloud base height distribution over Eastern China. Atmosphere 10(6):307. https://doi.org/10.3390/atmos10060307

Yu RC, Wang B, Zhou TJ (2004) Climate effects of the deep continental stratus clouds generated by the Tibetan Plateau. J Clim 17: 2702–2713. https://doi.org/10.1175/1520-0442(2004)017<2702:CEOTDC>2.0.CO;2

Yue Q, Fetzer EJ, Kahn BH, Wong S, Manipon G, Guillaume A, Wilson B (2013) Cloud-state-dependent sampling in AIRS observations based on CloudSat Cloud Classification. J Clim 26(21):8357–8377